Multidimensional Hydrogen Bond Dynamics in Salicylaldimine: Coherent Nuclear Wave Packet Motion versus Intramolecular Vibrational Energy Redistribution

M. Petković and O. Kühn*

Institut für Chemie, Physikalische und Theoretische Chemie, Freie Universität Berlin, Takustrasse 3, D-14195 Berlin, Germany

Received: June 13, 2003; In Final Form: July 30, 2003

The multidimensional wave packet dynamics of salicylaldimine following ultrafast infrared laser excitation of the OH-bending and -stretching vibrations is discussed. A seven-dimensional Cartesian reaction surface Hamiltonian in the diabatic representation is employed comprising the five skeleton normal modes which have the greatest influence on the in-plane hydrogen motion. For the numerical solution of the time-dependent Schrödinger equation the multiconfiguration time-dependent Hartree method is used. Coherent wave packet dynamics is observed after excitation of the OH-bending fundamental transition, whereas strong anharmonic mode couplings to the stretching transition cause intramolecular vibrational energy redistribution on a time scale of about 700 fs.

1. Introduction

Ever since hydrogen bonds (HBs) have been discovered, an effort has been made to understand their influence on the structural and dynamical properties of chemical and biological systems.[1−4] Infrared (IR) spectroscopy provides a valuable tool for characterizing HBs in terms of their vibrational states and the dipole transitions connecting them. As a consequence of HB formation, IR line shapes carry the signatures of anharmonicity and multidimensional mode coupling. Indeed, the available information provides the basis for a classification of HBs according to their strength.[5] The theoretical frame for this discussion is given by a simple Taylor expansion of the potential energy surface (PES) where only those anharmonicities are kept which are vital for a given situation.[6,7] For instance, for an HB of the type X−H···Y the Q_{X-H}-stretching vibrational coordinate will be coupled to the Q_{X-Y} coordinate which modulates the HB geometry. This coupling can be modeled by an interaction potential which is proportional to $Q_{X-H}{}^2Q_{X-Y}$. [5] Upon adiabatic separation of slow and fast motions, this leads to a picture of the PES for the motion along the slow coordinate in a given quantum state with respect to the fast coordinate. By analogy to vibronic transitions one expects a Franck−Condon like progression in the IR spectrum, which in the present case would correspond to combination transitions. With increasing system size the picture becomes more complex, that is, in principle many transitions can contribute to the line shape, and the ubiquitous Fermi resonance interaction between the bending overtone and the stretching fundamental X−H vibration may have a strong influence. From the perspective of nuclear wave packet dynamics in the excited X−H-stretching state, this increased complexity manifests itself in the transition from a simple coherent motion of the low-frequency coordinate to an intramolecular vibrational energy redistribution (IVR) process (for reviews on IVR see, for example, refs 8−10).

The problem of understanding the mechanism which leads to an X−H IR band shape is even more intricate in the condensed phase. Various models for incorporating the line broadening due to interactions with the solvent have been proposed,[11−19] but only the recent advances in ultrafast nonlinear IR spectroscopy[20−24] gave access to a microscopic understanding of the interplay between intramolecular and intermolecular broadening mechanisms. The intermolecular HB dynamics of liquid water, for instance, has been a challenge for decades, and recent efforts in experiment[20,22] and theory[17,18] advanced the subject considerably. On the other hand, intramolecular HBs are much better defined, and this was where quasi-coherent nuclear wave packet dynamics of an anharmonically coupled low-frequency mode were observed for the first time.[21] This provided a look behind a broad condensed phase IR line shape, revealing, for example, hidden combination transitions. The case of carboxy-deuterated phthalic acid monomethylester in CCl_4 was theoretically investigated using a density matrix formalism in combination with a classical molecular dynamics simulation.[19,25] It was found that a reasonable explanation especially of the ∼400 fs OD stretch vibrational relaxation time could be given in terms of a fourth-order solvent-assisted coupling mechanism.

Quantum dynamical wave packet propagations require the a priori knowledge of the PES. For the purpose of linear IR spectroscopy, in many cases a representation in terms of normal mode coordinates is appropriate,[26−28] whose selection for larger molecules can be based, for example, on the gradients of the PES in the vicinity of the primary mode which is optically excited.[19] Being interested in large amplitude motions, that is, proton transfer, one has to resort to reaction path/surface approaches. Here one uses a coordinate system which is adapted to the reaction and not biased toward a specific minimum configuration. The idea of a reaction path/surface Hamiltonian is to describe a few large amplitude motions accurately including all anharmonicities while treating the remaining degrees of freedom as orthogonal coupled oscillators.[29] A reaction path Hamiltonian formulated in terms of a one-dimensional intrinsic reaction coordinate[30] is not well-suited for proton transfer because this path may have a large curvature yielding considerable kinetic couplings. In some cases it might be appropriate to

* Corresponding author.

10.1021/jp035688r CCC: $25.00
Published on Web 09/12/2003

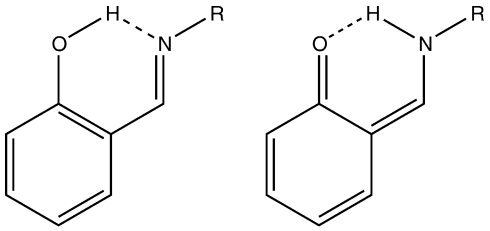

Figure 1. The two most stable tautomers of 2-hydroxybenzaldimine compounds; for salicylaldimine (SA) R = H.

use a straight-line reaction path instead which also facilitates a diabatic representation where all couplings are in the potential energy operator.[31] More flexibility, however, is provided by constructing a reaction surface in terms of several large amplitude coordinates such as the X−H−Y bond distances[32,33] or simple Cartesian coordinates.[34,35] The latter choice has the additional advantage of vanishing kinetic couplings, and it provides a straightforward connection to system-bath approaches used in condensed phase theory.[36,37]

Given a multidimensional reaction surface Hamiltonian, an appropriate method for wave packet propagation has to be chosen. Semiclassical methods have attracted considerable attention recently, despite the fact that quantum effects such as tunneling are accounted for only approximately.[38] Time-dependent self-consistent field theory in principle allows for an efficient high-dimensional quantum propagation,[39,40] but it is not well-adapted to situations such as proton transfer where anharmonic couplings change appreciably on the reaction surface.[41] Thus, a multiconfiguration time-dependent Hartree (MCTDH) approach[42] appears to be the method of choice for proton transfer. In passing we note that the combination of a reaction surface Hamiltonian with an MCTDH propagation has the additional advantage that for most coordinates the Hamiltonian has the separable form required for efficient implementation in the propagation scheme.[43]

In ref 43 we have combined an all-Cartesian reaction surface (CRS) Hamiltonian with an MCTDH wave packet propagation to investigate the laser-driven dynamics of the medium strong HB in deuterated phthalic acid monomethylester. Here only two modes coupled strongly to the OD-stretching motion giving rise to an IVR time scale of about 20 ps for this mode. The solvent-induced damping of the low-frequency X−Y type mode was about 1.7 ps which allowed for the observation of quasi-coherent wave packet dynamics. The question which motivated the present work can be stated as follows: Can we observe such wave packet dynamics also in systems having a somewhat weaker HB such that proton transfer between two stable configurations becomes possible? Particularly, we are interested in *asymmetric low-barrier* systems which in principle should allow for proton transfer triggered by a few IR photon process.[44,45] In fact, current ultrafast IR pulses are still too weak to enable multiphoton processes, and even nonlinear third-order spectroscopy requires a rather high extinction coefficient for the OH band.

In this respect 2-hydroxybenzaldimine compounds (Figure 1) seem to be well-suited. However, preliminary experimental results for *N*-phenylsalicylaldimine (R = Ph) in CCl_4 showed no indication of wave packet motion. Instead, an upper bound for the population decay after excitation at 2800 cm^{-1} was given as 0.9−1.3 ps.[46] In the following we will concentrate on the gas-phase dynamics of the simpler salicylaldimine (R = H) paying special attention to the issue of coherent wave packet dynamics vs IVR. In section 2 we outline the determination of

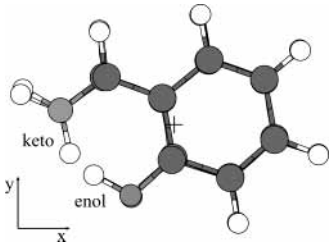

Figure 2. The two stationary configurations of SA (overlayed) as obtained at the DFT/B3LYP level of theory with a Gaussian 6-31+G(d,p) basis set. The origin of the molecule-fixed coordinate system corresponds to the center of mass and is marked by a cross. The axes (*x*, *y*) point along the principal axes of inertia for the more stable enol configuration.

TABLE 1: Parameters for the Stationary Points along the Enol−Keto Minimum Energy Path of Salicylaldimine As Obtained Using the DFT/B3LYP Method with a Gaussian 6-31+G(d,p) Basis Set[a]

	enol	TS	keto
ΔE_{SPE} (cm^{-1})	0.0	1940	1308
ΔE_{reorg} (cm^{-1})	0.0	3573	3112
R_{O-H} (Å)	0.999	1.293	1.729
R_{N-H} (Å)	1.716	1.194	1.038
R_{O-N} (Å)	2.611	2.406	2.579
d_x (D)	0.032	−1.042	−1.743
d_y (D)	2.847	3.522	3.842

[a] The components of the dipole moment *d* are given with respect to the coordinate system of the CRS Hamiltonian (cf. Figure 2).

a CRS Hamiltonian in the diabatic representation. Section 3 briefly reviews the MCTDH wave packet propagation method. Numerical results for a seven-dimensional model of salicylaldimine (SA) are given in section 4. Here we discuss the linear IR absorption spectrum and the dynamics after ultrafast IR laser excitation of the OH-bending and -stretching fundamental transitions. The paper is summarized in section 5.

2. Reaction Surface Hamiltonian

In the following we will focus on the simplest molecule from the 2-hydroxybenzaldimine family, that is, salicylaldimine (cf. Figure 1) because the computational effort increases significantly with the size of the R-group. We will construct an approximate but full-dimensional all-Cartesian reaction surface Hamiltonian for SA. In a first step we have determined the stationary points along the minimum energy path connecting the enol and the keto configuration using density functional theory (DFT) with the B3LYP exchange-correlation functional and a 6-31+G(d,p) basis set (all quantum chemistry calculations have been performed using the Gaussian 98 program package[47]). The optimized geometries of the planar enol and keto configuration are shown overlayed in Figure 2; characteristic parameters are compiled in Table 1. The more stable tautomer is the enol form because of the presence of the aromatic ring, whereas the less stable keto form possesses no aromatic character. Quantum chemical calculations of the stationary points for the enol−keto tautomerization of SA have been reported previously.[48−51] Specifically our results are in accord with ref 50 where it was established that the reaction is a proton transfer coupled to an electron transfer through the conjugated system.

Next we separate the total set of $3N = 48$ coordinates into those of the reactive H atom **x** and those of the substrate **Z**. The origin of the coordinate system is taken to be the center of mass at the enol configuration with the axes pointing along the principal axes of inertia (see Figure 2). This separation assumes that the substrate coordinates are well-described by a harmonic

approximation of the PES $V(\mathbf{x},\mathbf{Z})$ for a given $\mathbf{x}$. Thus, we can write for some configuration, $\mathbf{Z}^{(0)}(\mathbf{x})$, of the substrate atoms[34]

$$V(\mathbf{x},\mathbf{Z}) = V(\mathbf{x},\mathbf{Z}^{(0)}(\mathbf{x})) + \left.\frac{\partial V}{\partial \mathbf{Z}}\right|_{\mathbf{Z}^{(0)}(\mathbf{x})}(\mathbf{Z} - \mathbf{Z}^{(0)}(\mathbf{x})) + \frac{1}{2}(\mathbf{Z} - \mathbf{Z}^{(0)}(\mathbf{x}))\left.\frac{\partial^2 V}{\partial \mathbf{Z}\,\partial \mathbf{Z}}\right|_{\mathbf{Z}^{(0)}(\mathbf{x})}(\mathbf{Z} - \mathbf{Z}^{(0)}(\mathbf{x})) \quad (1)$$

In their original paper[34] Ruf and Miller discuss two different choices for $\mathbf{Z}^{(0)}(\mathbf{x})$; that is, either one uses some fixed reference configuration, $\mathbf{Z}^{(0)}(\mathbf{x}_{\mathrm{ref}}) \equiv \mathbf{Z}_{\mathrm{ref}}$, or the reference configuration is taken to be flexible, $\mathbf{Z}^{(0)}(\mathbf{x})$. In the language of proton-transfer reactions these choices resemble the sudden switch and the adiabatic approximation, respectively. It should be emphasized that as long as the harmonic approximation for the substrate atoms holds, there is no difference between these two choices as far as the *total* CRS Hamiltonian is concerned. However, for many systems the range of the validity of the harmonic approximation will be located in the vicinity of the minimum energy path on the adiabatic PES. Thus, fixing the substrate atoms at some reference configuration might carry the system too far into the anharmonic part of the PES. For the present enol−keto tautomerization this implies that although the PES in the vicinity of the enol configuration could be well-described by fixing the substrate at the respective stationary point, the harmonic approximation is likely to break down when crossing the reaction barrier. This is reflected in the fact that the relative energies of the enol, transition state (TS), and keto configuration on the full-dimensional Cartesian reaction surface do not match the fully relaxed values obtained from quantum chemistry.

Therefore, a more accurate description has to resort to a flexible reference. An obvious choice for the $\mathbf{Z}^{(0)}(\mathbf{x})$ is to perform a *partial* geometry optimization of all substrate coordinates for each value of $\mathbf{x}$. Although laborious, this procedure guarantees the correct energetics for the stationary points. Specifically, the single-point energies of the transition state and the keto tautomer, with respect to the enol form, which are 1940 and 1308 cm^{-1}, respectively (cf. Table 1), are well-reproduced.

Having calculated the forces and the Hessian matrix as a function of the reaction coordinates, one introduces normal mode coordinates for the substrate atoms according to the transformation $\mathbf{Z} - \mathbf{Z}^{(0)}(\mathbf{x}_{\mathrm{ref}}) = \mathbf{m}^{-1/2}\mathbf{U}\mathbf{Q}$. Note that the normal modes are defined with respect to some fixed reference configuration which in the present case is the enol minimum. Thus we have

$$\mathbf{Z} - \mathbf{Z}^{(0)}(\mathbf{x}) = \mathbf{Z}^{(0)}(\mathbf{x}_{\mathrm{ref}}) - \mathbf{Z}^{(0)}(\mathbf{x}) + \mathbf{m}^{-1/2}\mathbf{U}\mathbf{Q} \quad (2)$$

The geometries of the stationary points are planar; that is, there is no force on the H atom acting along the z direction. Therefore, we have chosen to restrict the large amplitude, anharmonic motion of the H atom to take place in the (x, y) plane. The z coordinate of the H atom is considered to belong to the harmonic substrate (for details see also ref 34). The coupling of this coordinate to the (x, y) reaction coordinates but also to the substrate is included in the Hessian matrix. Note that the appearance of this type of coupling is rather obvious because the corresponding out-of-plane-bending vibration is not proceeding perpendicular to the plane and its frequency is not constant when comparing the stationary points. Hence the substrate has total of $3N - 8 = 40$ degrees of freedom and the CRS Hamiltonian reads

$$\mathscr{H}_{\mathrm{CRS}} = T_{x,y} + V(x, y) - \mathbf{f}(x, y)\mathbf{Q} + \frac{1}{2}[\mathbf{P}^2 + \mathbf{Q}\mathbf{K}(x, y)\mathbf{Q}] \quad (3)$$

Here the potential $V(x, y)$, the forces $\mathbf{f}$, and the Hessian $\mathbf{K}$ follow straightforwardly from the normal mode transformation of eq 1. The linear coupling, $\propto\mathbf{f}(x, y)$, appears because of the fact that the large amplitude motion does not take place along the minimum energy path. It is the force which acts on the substrate normal mode oscillators to push them back into their (locally) relaxed configuration. The mixing between the substrate normal modes induced by the reaction coordinates is described by the quadratic coupling, which is proportional to the transformed Hessian, $\mathbf{K}(x, y)$. Notice that because of the large mass ratio between the H atom and the substrate the center of mass as well as the orientation of the principal axes of inertia do not change appreciably during the proton transfer; that is, for the present purpose we can neglect the coupling to the external motions and retain the simple form of the kinetic energy operator.

We have determined $\mathscr{H}_{\mathrm{CRS}}$ from a total of 205 quantum chemistry points in the (x, y) plane which were scattered to cover the reaction surface valley. The data have been fitted on a regular grid employing a bivariate, locally quintic interpolant. The effective potential $V(x, y)$ is shown in Figure 3A. The right valley corresponds to the enol form (i.e., it represents the global minimum), and the left one corresponds to the less stable keto tautomer. It is noteworthy that the keto valley is comparatively shallow.

In principle, eq 3 provides a full-dimensional description of the proton motion in SA. Of course, not all modes are strongly coupled to the reaction coordinate, and it is to be expected that there is some hierarchy of couplings by which the importance of particular substrate modes can be judged. The most obvious classification is in terms of in-plane and out-of-plane modes; for the latter $f_i(x, y)$ vanishes. In the spirit of our two-dimensional reaction coordinate model we restrict our considerations to the 25 in-plane substrate modes. Their coupling to the reaction coordinates can be characterized by the total reorganization energy

$$\Delta E_{\mathrm{reorg}}(x, y) = \frac{1}{2}\mathbf{f}(x, y)[\mathbf{K}(x, y)]^{-1}\mathbf{f}(x, y) \quad (4)$$

which in the present case is 3573 and 3112 cm^{-1} for the TS and the keto configuration, respectively. Notice that subtracting these values from $V(x, y)$ at the stationary points reproduces the energetics of the fully relaxed PES (see Table 1). As a compromise between accuracy and feasibility of the numerical solution of the Schrödinger equation, we have chosen the five most important in-plane substrate modes. They account for approximately 80% and 46% of the total reorganization energy at the TS and keto configuration. The contributions of the different modes are listed in Table 2 neglecting mode coupling, that is, $\Delta E_{\mathrm{reorg},\,i} = f_i^2/(2K_{ii})$. For the remaining in-plane as well as for the out-of-plane modes, we assume that they are frozen at their reference enol configuration, because none of them are particularly strongly coupled to the reaction coordinate.

The normal mode displacements of the selected modes for the enol reference point are shown in Figure 4; their frequencies at the enol configuration are given in Table 2. As expected, these modes modify the H bond geometry. We notice, however, that the effect of modes (ν_4, ν_{14}) and of modes (ν_6, ν_{26}, ν_{30}) is different. The former are of the gating type because they reduce the N−O distance and thus promote proton transfer. In contrast, the latter three modes are directly related to the rearrangement of single and double bonds which takes place during enol−keto tautomerization (cf. Figure 1). In the context of proton

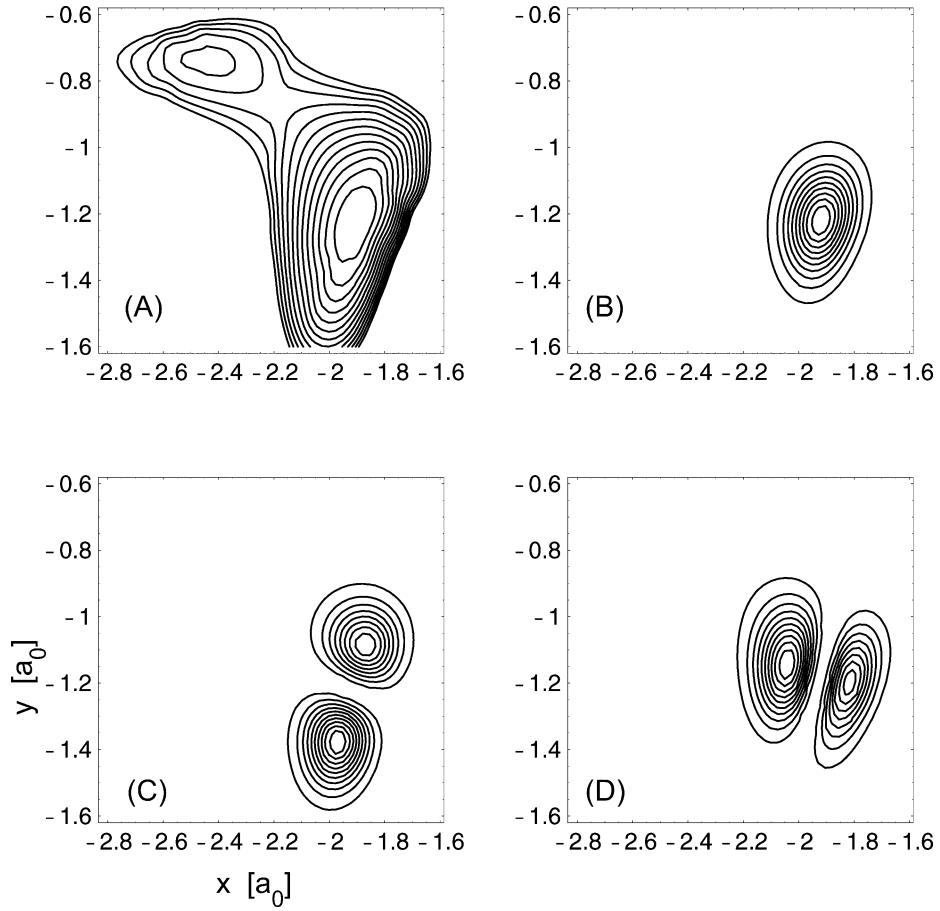

Figure 3. (A) Potential energy surface, $V(x, y)$ for the reaction coordinates corresponding to the in-plane H motion in SA with the substrate normal modes fixed at their equilibrium positions (see Figure 2). The contours are given in steps of 500 cm^{-1} up to 6500 cm^{-1}. The wave functions for the ground state (B), the lowest bending excitation (C), and stretching excitation (D) are given as well. They have been calculated on a 64 × 64 grid in the interval (in a_0) $x \in [3.3:1.3]$ and $y \in [-2.0:-0.3]$ using the WavePacket 3.0 program.[57]

TABLE 2: Mode Number (*i*), Mode Frequencies at the Enol Configuration of SA, and Approximate Reorganization Energies for Each Mode at the Transition State (TS) and Keto Configuration As Obtained Using the DFT/B3LYP Method with a Gaussian 6-31+G(d,p) Basis Set

		ΔE_{reorg} (cm^{-1})	
i	ω_i (cm^{-1})	TS	keto
4	336	1317	3
6	451	771	88
14	861	1100	55
26	1333	114	635
30	1513	263	755

tunneling between equivalent minima, this type of mode is usually referred to as being of the "linear-coupling" type.[52] But notice that this classification is based on symmetry considerations which do not apply for the present case of nonequivalent enol and keto configurations.

We proceed by defining *diabatic* states, $\phi_\alpha(x, y) = \langle x, y|\alpha\rangle$, with respect to the reaction coordinate according to the Schrödinger equation

$$[T_{x,y} + V(x, y)]\,\phi_\alpha(x, y) = E_\alpha\,\phi_\alpha(x, y) \tag{5}$$

This definition implies that only the hydrogen motion is accounted for and all relevant substrate modes are frozen at their equilibrium value $\mathbf{Q} = 0$ corresponding to the enol configuration. The motivation for introducing the diabatic representation is twofold: First, the diabatic states are rather useful zero-order states for classifying the nature of the IR transitions in terms of OH-bending and -stretching transitions. This is illustrated in Figure 3 where we show the respective wave functions for the ground state (panel B), the first excited state (OH bending, panel C), and the second excited state (OH stretching, panel D). The excitation energies for the lowest 10 diabatic states are given in Table 3. The second point is of a more technical nature. It is to be expected that the harmonic approximation for the substrate modes breaks down far away from the reaction surface valley. Thus, it is rather difficult to obtain reliable information about the substrate modes on the full range of coordinates shown in Figure 3A. In practice this means, for example, that the Hessian will have several negative eigenvalues. However, from Figure 3 it is also clear that the diabatic wave functions, which can be obtained on a much larger grid than a useful Hessian, are localized in the relevant reaction valley region where the substrate mode potential can reliably be obtained.

In the diabatic representation the CRS Hamiltonian for the reduced seven-dimensional model is given by

$$\mathscr{H}_{\mathrm{CRS}}^{\mathrm{diab}} = \frac{1}{2}\mathbf{P}^2 + \sum_{\alpha,\beta}[U_\alpha(\mathbf{Q})\delta_{\alpha\beta} + V_{\alpha\beta}(\mathbf{Q})(1 - \delta_{\alpha\beta})]|\alpha\rangle\langle\beta| \tag{6}$$

where the diabatic potential energy curves have been defined as

$$U_\alpha(\mathbf{Q}) = E_\alpha - \mathbf{f}_{\alpha\alpha}\mathbf{Q} + \frac{1}{2}\mathbf{Q}\mathbf{K}_{\alpha\alpha}\mathbf{Q} \tag{7}$$

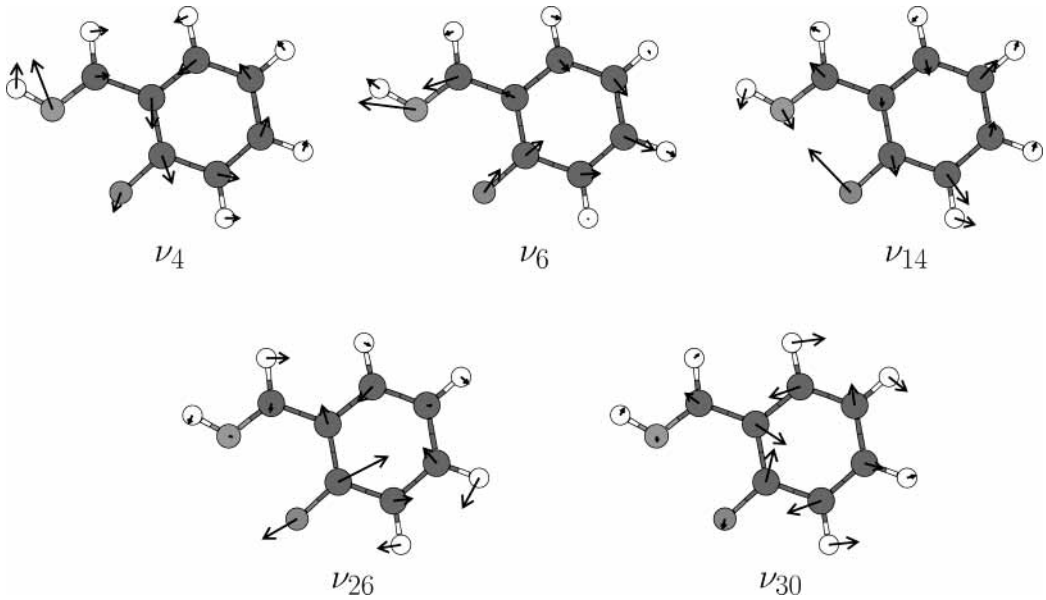

Figure 4. Normal mode displacement vectors at the enol configuration for the five most important in-plane substrate modes. The mode frequencies and reorganization energies are compiled in Table 2.

TABLE 3: Number of Single-Particle Functions per Diabatic State, $|\alpha\rangle$, and the Grid Dimension ($\min(Q_i)/\max(Q_i)$) Used for the MCTDH Wave Packet Propagation for the Substrate Modes Shown in Figure 4

	diabatic state (α)										
i	1 (0[a])	2 (1416[a])	3 (2612[a])	4 (2811[a])	5 (3806[a])	6 (4063[a])	7 (4253[a])	8 (4702[a])	9 (5140[a])	10 (5450[a])	grid[b]
4	5	4	4	4	4	3	3	3	2	2	−170/170
6	5	4	4	4	4	3	3	3	2	2	−130/130
14	5	4	4	4	4	3	3	3	2	2	−70/70
26	4	3	3	3	3	3	3	3	2	2	−45/45
30	4	3	3	3	3	3	3	3	2	2	−40/40

[a] The transition frequency in cm^{-1} is given in parentheses. [b] Units are $a_0\sqrt{\text{amu}\, m_e}$.

and the coupling between the diabatic states is given by

$$V_{\alpha\beta}(\mathbf{Q}) = -\mathbf{f}_{\alpha\beta}\mathbf{Q} + \frac{1}{2}\mathbf{Q}\mathbf{K}_{\alpha\beta}\mathbf{Q} \tag{8}$$

Here $\mathbf{f}_{\alpha\beta}$ and $\mathbf{K}_{\alpha\beta}$ are the diabatic state matrix elements of the forces and the Hessian, respectively. As an example we show diabatic potential energy curves $U_\alpha(Q_{14})$ for mode ν_{14} in Figure 5. The lowest state corresponds to the global minimum, enol tautomer, and curve 5 to a diabatic state localized in the left minimum (keto form). As indicated earlier, the second state represents the bending and the third state the stretching fundamental vibration. The fourth state is the second excited bending vibration (overtone). This means that the first four states are localized in the *enol well* (−OH), whereas the fifth state has a *keto character* (−NH). For that reason the fifth curve has the greatest shift with respect to the ground state, which implies a strong force acting on this mode in the keto valley.

In the following we investigate the dynamics triggered by an ultrafast IR laser pulse excitation. The matter−field interaction is described (within the dipole approximation) by a time-dependent interaction Hamiltonian, which contains the dipole moment operator $\mathbf{d}(x, y)$ in the diabatic representation

$$\mathscr{H}_{\text{field}}(t) = -\sum_{\alpha,\beta} |\alpha\rangle \mathbf{d}_{\alpha\beta}\, \epsilon(t) \langle\beta| \tag{9}$$

For the laser field we will assume the following form

$$\epsilon(t) = \hat{\mathbf{e}}\epsilon_0\, \Theta(t)\, \Theta(\tau - t)\, \sin^2(\pi t/\tau)\, \cos(\Omega t) \tag{10}$$

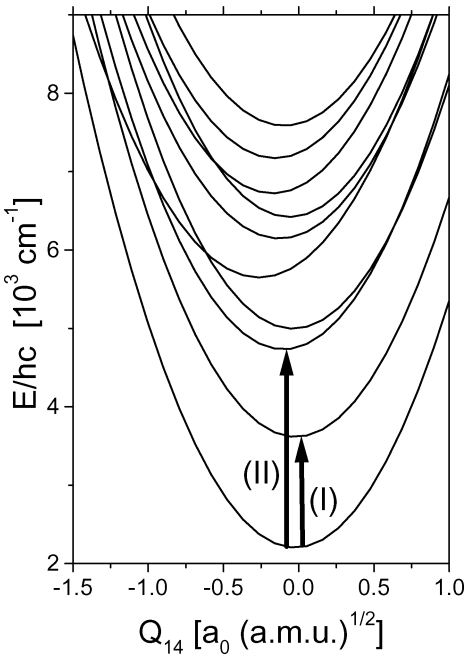

Figure 5. Diabatic potential energy curves $U_\alpha(Q_{14})$ for mode ν_{14}. The arrows schematically show the laser pulse excitation of the bending (I) and stretching (II) fundamental transitions. The actual excitation frequencies have been chosen according to the linear IR spectrum which contains the effect of diabatic state and mode−mode coupling.

where $\hat{\mathbf{e}}$ and ϵ_0 represent the polarization and amplitude of the field, respectively, τ represents the duration of the pulse, and

Ω represents its center frequency. The dipole moment vector is oriented in the plane of the molecule, that is, $\mathbf{d}(x, y) = (d_x(x, y), d_y(x, y), 0)$. In the vicinity of the enol configuration the gradient of the dipole for $d_x(x, y)/d_y(x, y)$ points approximately along the x/y axis (not shown). Notice that we have tacitly assumed that the field interacts with the reaction coordinates only. This point will be further discussed in section 4.

To summarize this section, the total CRS Hamiltonian can be written as

$$\mathscr{H}_{\mathrm{tot}}(t) = \mathscr{H}^{\mathrm{diab}}_{\mathrm{CRS}} + \mathscr{H}_{\mathrm{field}}(t) \tag{11}$$

Both contributions are readily incorporated into the MCTDH wave function propagation which will be outlined in the next section.

3. MCTDH Wave Packet Dynamics

The time-dependent Schrödinger equation for the CRS Hamiltonian, eq 11, has been solved using the MCTDH method, as detailed in ref 42. Here the wave function is expanded in the set of diabatic states $|\alpha\rangle$

$$|\Psi\rangle = \sum_{\alpha=1}^{\nu} \psi_\alpha |\alpha\rangle \tag{12}$$

where the coefficients are represented as linear combinations of Hartree products of one-dimensional time-dependent single-particle functions φ,

$$\psi_\alpha(Q_1, ..., Q_f, t) = \sum_{j_1^{(\alpha)}=1}^{n_1^{(\alpha)}} \cdots \sum_{j_f^{(\alpha)}=1}^{n_f^{(\alpha)}} A^{(\alpha)}_{j_1^{(\alpha)},\ldots,j_f^{(\alpha)}}(t) \prod_{\kappa=1}^{f} \varphi^{(\alpha,\kappa)}_{j_\kappa^\alpha}(Q_\kappa, t) = \sum_{J_\alpha} A^\alpha_{J\alpha}\, \Phi^\alpha_{J\alpha} \tag{13}$$

Here Q_i are the substrate normal mode coordinates and $A^\alpha_{J\alpha}(t)$ are time-dependent expansion coefficients for the Hartree product $\Phi^\alpha_{J\alpha}$. Equation 13 corresponds to the so-called multiset formulation, where different sets of single-particle functions have been defined for each diabatic state.[42,53] In the simulation we employed 10 diabatic states, with the numbers of single-particle functions per level for each mode compiled in Table 3. Each single-particle function is expanded using a fast Fourier transform primitive basis representation with 32 grid points (see also Table 3).

Using the Dirac−Frenkel variational principle, one arrives at a system of coupled equations of motion for the expansion coefficients and the single-particle functions entering eq 13. The numerical solution requires the evaluation of multidimensional integrals to obtain a mean-field Hamiltonian matrix. Here it is important to emphasize that the CRS Hamiltonian, eq 11, is separable with respect to the substrate modes which enables a very efficient integral evaluation.[43] The propagation of a wave function has been performed using the Heidelberg MCTDH package.[54] We employed a variable mean-field method using the Adams−Bashforth−Moulton predictor-corrector integrator of sixth-order with an error tolerance of 10^{-7} and an initial step size 0.01 fs.[42]

4. Numerical Results

4.1. Linear IR Absorption Spectrum. Before presenting laser-driven dynamics, we will focus on the stationary linear IR absorption spectrum which can be obtained from the dipole autocorrelation function according to (n_{mol}: volume density)[36]

$$I(\omega) = \frac{4\pi\omega n_{\mathrm{mol}}}{3\hbar c} \sum_{i=x,y} \mathrm{Re} \int_0^\infty \mathrm{d}t\, \mathrm{e}^{\mathrm{i}(\omega-\omega_0)t-\Gamma t} \times \langle \Psi_0 | d_i(x, y) \mathrm{e}^{-\mathrm{i}\mathscr{H}^{\mathrm{diab}}_{\mathrm{CRS}} t/\hbar}\, d_i(x, y) | \Psi_0 \rangle \tag{14}$$

Here $\hbar\omega_0$ stands for the energy of the ground state $|\Psi_0\rangle$ (for simplicity we assume that the temperature is $T = 0$ K). Furthermore, a phenomenological damping parameter Γ has been introduced to account for the effect of lifetime broadening. The latter will be dominated by the interaction with, for example, a solvent and may in principle depend on the type of motion (bending, stretching). Because we are not aiming at a microscopic description of solvent effects, Γ is solely used to facilitate the calculation of the Fourier transform of a finite-time (3 ps) correlation function in eq 14. In Figure 6 we show the separate contributions from the d_x and d_y vector components of the dipole moment. Inspection of Figure 3 already indicates that the excitations of the bending and stretching transitions will be dominated by the d_y and d_x components of the dipole moment. Indeed, there is a clear separation of the two dipole orientations: The d_y component gives mostly the bending fundamental transition around 1400−1500 cm^{-1}, whereas the d_x component is responsible for the broad band from 2200 to 2800 cm^{-1} corresponding to the fundamental stretching transition. Notice that experimental spectra have been recorded, but not fully assigned, for SA−Ph in CCl_4 solution only.[46] Here one finds two broad bands around 2600 and 2750 cm^{-1} which disappear upon deuteration. Given some solvent-induced broadening mechanism, this correlates well with the OH-stretching type transition in Figure 6. Furthermore, the region around 1400 cm^{-1} shows a double peak which almost disappears in the deuterated species. In view of Figure 6 this might be related to the OH-bending fundamental transition.

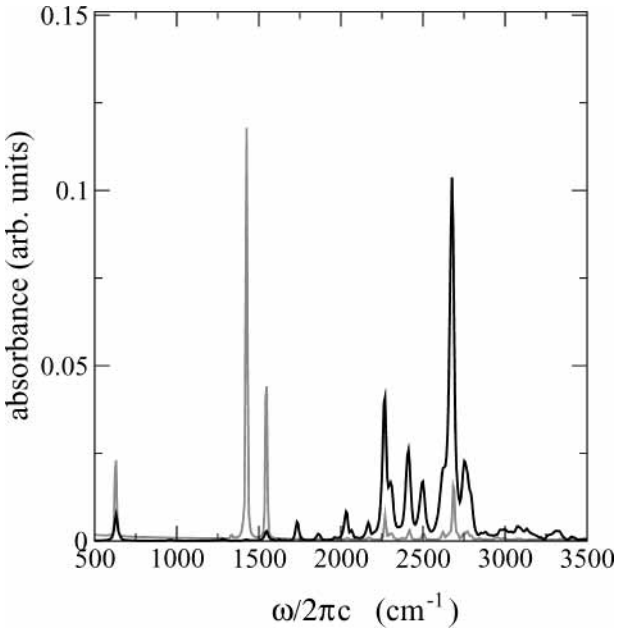

Figure 6. Linear absorption spectrum, eq 14, for the 7D model of SA. The separate contributions from the d_y (gray) and d_x (black) components of the dipole moment are shown. The spectra have been obtained from a 3 ps wave function propagation. For the damping parameter we have taken $\Gamma^{-1} = 2.5$ ps (d_y) and 0.5 ps (d_x), merely for visual clarity.

Already at the level of the linear absorption the difference between bending and stretching fundamental transitions becomes

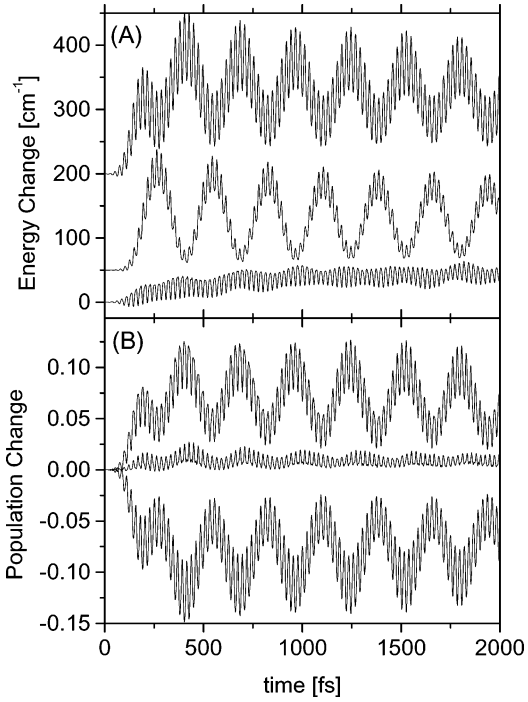

Figure 7. (A) Energy change with respect to time zero for the two reaction coordinates, $E_{xy}(t)$ (eq 15), mode ν_{30}, $E_{Q_{30}}(t)$ (eq 16), and the combined other four substrate modes (from top, curves have been vertically offset). (B) Difference population, eq 17, with respect to time zero for selected diabatic states: ΔP_1, $\sum_{\alpha=3,10}\Delta P_\alpha$, and ΔP_2 (curves from bottom to top). The laser pulse was tuned in resonance with the bending fundamental transition taking into account only the *y* component of the dipole operator. The pulse parameters are $\epsilon_0 = 4 \times 10^{-3} E_h/(ea_0)$, $\Omega/(2\pi c) = 1425$ cm^{-1}, $\tau = 260$ fs.

apparent. The bending transition is found to develop a dominant double-peak structure due to a resonance with the fundamental transition of the substrate mode ν_{30}. For the stretching fundamental transitions we have a rather strong coupling to *all* substrate modes as well as a mixing with the bending overtone transition (cf. Figure 5). This renders an assignment in terms of single zero-order states meaningless.

In general it is to be expected that the inclusion of the substrate modes in the dipole operator may change the IR spectrum quantitatively and thus the initial conditions for the dynamics after excitation. However, in the spirit of the harmonic approximation this would mainly affect the fundamental transitions involving those modes. In this respect it is interesting to note that, for example, for the OH-bending region the correct behavior upon deuteration is reproduced (see above). This implies that the ν_{30} fundamental transition mostly "borrows" oscillator strength from the OH-bending vibration via anharmonic coupling.

4.2. OH-Bending Vibration. In Figure 7 we show the dynamics of our seven-dimensional CRS Hamiltonian after ultrafast excitation of the OH-bending fundamental transition ($\Omega/(2\pi c) = 1425$ cm^{-1}, cf. Figure 5). After the pulse was switched off ($\tau = 260$ fs), the wave function was propagated so that the total propagation lasted 2000 fs. The maximum natural orbital population of the single-particle function giving the smallest contribution was 3.7375×10^{-3} for mode ν_4 of state $|\alpha = 1\rangle$.

Figure 7A contains the expectation values for the energy of the reaction coordinates

$$E_{xy}(t) = \sum_\alpha E_\alpha \langle\Psi(t)|\alpha\rangle\langle\alpha|\Psi(t)\rangle \tag{15}$$

as well as the energy of the uncoupled substrate modes

$$E_{Q_i}(t) = \frac{1}{2}\sum_\alpha \langle\Psi(t)|\alpha\rangle[P_i^2 + \langle\alpha|K_{ii}(x,y)|\alpha\rangle Q_i^2]\langle\alpha|\Psi(t)\rangle \tag{16}$$

As to be expected from the linear spectrum, the spectrally broad pulse excites a coherent superposition of the bending and ν_{30} fundamental transitions. Viewed in terms of the energy exchange between the reaction coordinates and the substrate mode, this is reflected in the slow modulations which have opposite phase for $E_{xy}(t)$ and $E_{Q_{30}}(t)$ in Figure 7A. The other four modes are only very weakly coupled to this dynamics. In fact their energy content is only slightly increasing during the first 2 ps which comes along with the overall decrease of the energy in the H atom's motion. This reflects IVR which under the present conditions is very inefficient. In fact a single-exponential fit of the slow decay of $E_{xy}(t)$ gives a time scale of about 5.2 ps.

It is instructive to explore the dynamics in terms of the populations of the diabatic states defined as

$$P_\alpha(t) = \langle\Psi(t)|\alpha\rangle\langle\alpha|\Psi(t)\rangle \tag{17}$$

The population change with respect to time zero, $\Delta P_\alpha(t) = P_\alpha(t) - P_\alpha(0)$, is shown in Figure 7B.

Because of the excitation conditions, only the two lowest states are becoming appreciably excited. The fact that the OH-bending vibration and the substrate mode ν_{30} are strongly coupled manifests itself in the opposite phase oscillations of the population changes ΔP_1 and ΔP_2. This implies that the ν_{30} fundamental transition belongs to the potential energy surface for the diabatic ground state of the reaction coordinates. Again we notice a very slow recovery of the ground state population change due to IVR processes.

The participation of mainly two states in Figure 7 suggests an interpretation of the slow opposite phase modulation in terms of a two-state model. Here it is known[36] that the population exchange between two states takes place with a frequency $(\Delta\epsilon^2 + 4V^2)^{1/2}/(2\hbar)$, where $\Delta\epsilon$ and V are the detuning and the coupling between the states, respectively. In the present case the detuning between the zero-order states is about 100 cm^{-1} which gives a value of 70 cm^{-1} for the state-coupling V factor to reproduce the modulation frequency of 280 fs.

4.3. OH-Stretching Vibration. The situation is rather different when exciting in the region of the OH-stretching fundamental transition. In Figure 8A we show the change in energy expectation values which follow after an excitation at $\Omega/(2\pi c) = 2680$ cm^{-1}. The spectral width of the pulse (175 cm^{-1}) is sufficient to excite most of the broad band shown in Figure 6. As can be seen from Figure 8A, this implies that *all* substrate normal modes become almost equally excited. As a consequence the energy contained in the reaction coordinates quickly relaxes. That means IVR is very effective, and the related time scale obtained from a single-exponential fit of $E_{xy}(t)$ is about 720 fs. We note that there is a slow modulation with a period of about 400 fs superimposed on the overall decay of $E_{xy}(t)$. This cannot be attributed to the interaction with a *single* substrate mode so as to resemble wave packet motion in the excited diabatic state potential. Inspecting the total energy content of all substrate modes which is also shown in Figure 8A, we observe the same slow modulation; that is, this is related to a time scale given by the coupling between the reaction coordinates and the substrate as a whole.

This point can be further clarified by inspecting the diabatic state populations shown in Figure 8B. First we notice that

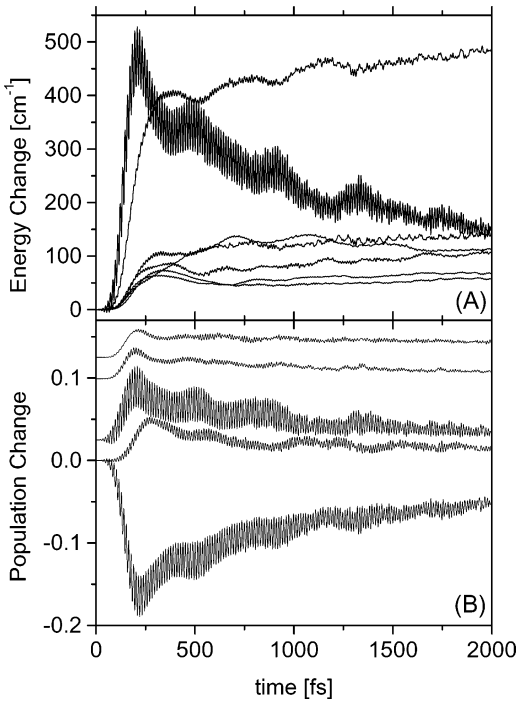

Figure 8. (A) Energy change with respect to time zero for all substrate modes, the two reaction coordinates, as well as modes ν_{14}, ν_{26}, ν_{30}, ν_4, and ν_6 (from top of right-hand side, cf. eqs 15 and 16). (B) Difference population, eq 17, with respect to the time zero for the lowest 10 diabatic states: ΔP_1, ΔP_2, ΔP_3, ΔP_5, and $\sum_{\alpha=4,6-10}\Delta P_\alpha$ (curves from bottom to top, upper curves are vertically offset). The laser pulse was tuned in resonance with the stretching fundamental transition region taking into account only the x component of the dipole operator. The pulse parameters are $\epsilon_0 = 4 \times 10^{-3} E_h/(ea_0)$, $\Omega/(2\pi c) = 2680$ cm^{-1}, $\tau =$ 260 fs.

essentially the population of the lowest three states is changed, although higher excited states are populated as well, most notably the diabatic state $|\alpha = 5\rangle$ which corresponds to the keto configuration. From the dynamics of the three lowest diabatic states we can draw the following conclusions: (i) Because both states $|\alpha = 3\rangle$ and $|\alpha = 2\rangle$ are populated already by the laser pulse, it follows that part of the OH-stretching band comes from contribution of vibrational states which belong to the diabatic OH-bending state. (ii) The low-frequency modulations seen in Figure 8A is also found in the population dynamics of these three states. In fact the modulation in ΔP_3 has an opposite phase with respect to the modulation of ΔP_1 and ΔP_2. This suggests that this slow modulation comes from a quasi-coherent population exchange between the stretching state $|\alpha = 3\rangle$ and substrate mode states which present energetically accessible excitations in the ground *and* bending diabatic PES $U_{\alpha=1,2}(\mathbf{Q})$. It is intriguing to see that despite the complexity a modulation in the average energy can be observed over three periods.

5. Summary

We have investigated the intramolecular vibrational dynamics of salicylaldimine, triggered by an ultrafast IR laser pulse. Thereby we combined a seven-dimensional diabatic reaction surface Hamiltonian including the most relevant in-plane vibrational modes with a numerically exact MCTDH wave packet propagation. After assignment of the linear IR spectrum to the OH-bending (1400−1500 cm^{-1}) and OH-stretching (2200−2800 cm^{-1}) fundamental transitions, two excitation conditions have been considered which lead to rather different dynamics. (i) For OH-bending excitation the dynamics during the first 2 ps is governed by the exchange of energy between the fundamental transitions of the OH-bending and a single nearly resonant substrate mode (ν_{30}). The energy flow (IVR) into the other modes is rather slow with an estimated time scale of about 5.2 ps. (ii) For OH-stretching excitation the transition is strongly coupled to all substrate normal modes giving rise to a subpicosecond (720 fs) IVR process in rather good agreement with the preliminary experimental result.[46] However, we have to emphasize that for a conclusive comparison more experimental data are needed. Despite this fast energy redistribution, the analysis of the energy content of the different degrees of freedom and the population changes in the diabatic states showed some slow (400 fs) modulation for about three periods. This has been explained by a population flow between the OH-stretching diabatic state and the vibrationally excited states of the substrate normal modes within the ground and bending state potential energy surfaces.

The dynamics of the present system apparently is rather different from that of the previously studied phthalic acid monomethylester.[19,25,43] In that case the coupling of the OD-stretching vibration to two specific modes was very pronounced and vibrational wave packet dynamics with respect to a low-frequency mode which modulates the HB geometry could be observed. However, this system has only a single minimum potential energy surface. The low-barrier double-minimum situation in salicylaldminine leads to a more anharmonic potential energy surface with considerable mode couplings. Interestingly, we predict a slow modulation of the excited-state dynamics which, however, should not be confused with wave packet dynamics with respect to a particular mode. In fact all substrate modes in our model have frequencies which are much too high to facilitate an efficient direct excitation of a Franck−Condon like progression with available IR lasers.

The IR dynamics and spectroscopy of HBs are of fundamental interest on their own. Looking ahead, one might speculate whether the active control of proton motion by means of specially designed IR laser pulses is possible. Here different scenarios have been suggested based on low-dimensional model systems.[45,55,56] The present example of salicylaldimine gives some insight into the feasibility of IR laser control. Suppose the goal would be to trigger the enol−keto tautomerization. In terms of the diabatic states this would imply a transition between states $|\alpha = 1\rangle$ and $|\alpha = 5\rangle$ (see Figure 3). First we notice that this state is not easily accessible by a direct excitation because of small dipole matrix elements caused by the localization of the initial and final states in different potentials wells. Note, however, that there is a small population of this state upon excitation of the OH-stretching transition because of the mixing of the diabatic states. Looking for a two-step excitation mechanism, we note that the OH-bending and -stretching states are almost equivalent for the first step as far as the transition dipole matrix elements are concerned. However, the rather fast IVR in the OH-stretching state suggests an initial bending excitation to be more appropriate. The potential energy surface of the final state is considerably shifted with respect to the bending state potential as seen in Figure 3. This implies that even in the one-dimensional picture shown in this figure the wave packet promoted to the $|\alpha = 5\rangle$ state will start to move until it reaches a region where $U_5(\mathbf{Q})$ crosses with $U_4(\mathbf{Q})$. This would cause a population flow between the two states, and IVR would most likely diminish the control yield considerably. Thus, the second pulse should not only excite the product state but at the same time stabilize it, that is, drive the wave packet toward the minimum configuration of the potential surface $U_5(\mathbf{Q})$. It

goes without saying that the picture is more complicated than that shown in Figure 5 because of the mode coupling. Nevertheless this discussion illustrates that simple sequences of pulses with fixed carrier frequencies most likely will not work and more elaborate pulse shapes have to be utilized.

Acknowledgment. This work has been financially supported by the Deutsche Forschungsgemeinschaft through the Sfb 450 and the Fonds der Chemischen Industrie (O.K.). The authors gratefully acknowledge stimulating discussions with J. Manz (FU Berlin) and J. Dreyer, K. Heyne, E. T. J. Nibbering, and T. Elsaesser from the Max Born Institute Berlin.

References and Notes

(1) *The Hydrogen Bond Theory*; Schuster, P., Zundel, G., Sandorfi, C., Eds.; North Holland: Amsterdam, 1976.
(2) Jeffrey, G. A. *Hydrogen Bonding*; Oxford University Press: New York, 1997.
(3) *Theoretical Treatments of Hydrogen Bonding*; Hadži, D., Ed.; Wiley & Sons: Chichester, U.K., 1997.
(4) Scheiner, S. *Hydrogen Bonding*; Oxford University Press: New York, 1997.
(5) Bratos, S.; Leicknam, J.-C.; Gallot, G.; Ratajczak, H. In *Ultrafast Hydrogen Bond Dynamics and Proton Transfer Processes in the Condensed Phase*; Elsaesser, T., Bakker, H. J., Eds.; Kluwer Academic Publishers: Dordrecht, The Netherlands, 2002; p 5.
(6) Henri-Rousseau, O.; Blaise, P. *Adv. Chem. Phys.* **1998**, *103*, 1.
(7) Henri-Rousseau, O.; Blaise, P.; Chamma, D. *Adv. Chem. Phys.* **2002**, *121*, 241.
(8) Quack, M. *Annu. Rev. Phys. Chem.* **1990**, *41*, 839.
(9) Uzer, T. *Phys. Rep.* **1991**, *199*, 73.
(10) Gruebele, M.; Bigwood, R. *Int. Rev. Phys. Chem.* **1998**, *17*, 91.
(11) Robertson, G. N.; Yarwood, J. *Chem. Phys.* **1978**, *32*, 267.
(12) Marechal, Y.; Witkowski, A. *J. Chem. Phys.* **1968**, *48*, 3697.
(13) Rösch, N.; Ratner, M. A. *J. Chem. Phys.* **1974**, *61*, 3344.
(14) Bratos, S. *J. Chem. Phys.* **1975**, *63*, 3499.
(15) Bratos, S.; Ratajczak, H. *J. Chem. Phys.* **1982**, *76*, 77.
(16) Rey, R.; Hynes, J. T. *J. Chem. Phys.* **1996**, *104*, 2356.
(17) Lawrence, C. P.; Skinner, J. L. *J. Chem. Phys.* **2002**, *117*, 5827.
(18) Rey, R.; Moller, K. B.; Hynes, J. T. *J. Phys. Chem. A* **2002**, *106*, 11993.
(19) Kühn, O. *J. Phys. Chem. A* **2002**, *106*, 7671.
(20) Woutersen, S.; Emmerichs, U.; Bakker, H. J. *Nature* **1997**, *278*, 658.
(21) Stenger, J.; Madsen, D.; Dreyer, J.; Nibbering, E. T. J.; Hamm, P.; Elsaesser, T. In *Ultrafast Phenomena XII*; Elsaesser, T., Mukamel, S., Murnane, M., Scherer, N., Eds.; Springer Series in Chemical Physics; Springer Publishing: New York, 2000; p 542.
(22) Stenger, J.; Madsen, D.; Hamm, P.; Nibbering, E. T. J.; Elsaesser, T. *Phys. Rev. Lett.* **2001**, *87*, 027401.
(23) Stenger, J.; Madsen, D.; Dreyer, J.; Nibbering, E. T. J.; Hamm, P.; Elsaesser, T. *J. Phys. Chem. A* **2001**, *105*, 2929.
(24) Stenger, J.; Madsen, D.; Dreyer, J.; Hamm, P.; Nibbering, E. T. J.; Elsaesser, T. *Chem. Phys. Lett.* **2002**, *354*, 256.
(25) Kühn, O.; Naundorf, H. *Phys. Chem. Chem. Phys.* **2003**, *5*, 79.
(26) Pochert, J.; Quack, M.; Stohner, J.; Willeke, M. *J. Chem. Phys.* **2000**, *113*, 2719.
(27) Emmeluth, C.; Suhm, M. A.; Luckhaus, D. *J. Chem. Phys.* **2003**, *118*, 2242.
(28) Doslic, N.; Kühn, O. *Z. Phys. Chem.*, in press.
(29) Kraka, E. In *Encyclopedia Computational Chemistry*; von Ragué-Schleyer, P., Ed.; Wiley & Sons: New York, 1998; p 2437.
(30) Miller, W. H.; Handy, N. C.; Adams, J. E. *J. Chem. Phys.* **1980**, *72*, 99.
(31) Miller, W. H.; Ruf, B. A.; Chang, Y.-T. *J. Chem. Phys.* **1988**, *89*, 6298.
(32) Carrington, T.; Miller, W. H. *J. Chem. Phys.* **1984**, *81*, 3941.
(33) Shida, N.; Barbara, P. F.; Almlöf, J. E. *J. Chem. Phys.* **1989**, *91*, 4061.
(34) Ruf, B. A.; Miller, W. H. *J. Chem. Soc., Faraday Trans. 2* **1988**, *84*, 1523.
(35) Naundorf, H.; Organero, J. A.; Douhal, A.; Kühn, O. *J. Chem. Phys.* **1999**, *110*, 11286.
(36) May, V.; Kühn, O. *Charge and Energy Transfer Dynamics in Molecular Systems*; Wiley-VCH: Berlin, 2000.
(37) Xu, R.; Yan, Y.-J.; Kühn, O. *Eur. J. Phys. D* **2002**, *19*, 293.
(38) Guallar, V.; Gherman, B. F.; Miller, W. H.; Lippard, S. J.; Friesner, R. A. *J. Am. Chem. Soc.* **2002**, *124*, 3377.
(39) Hammes-Schiffer, S. *Faraday Discuss.* **1998**, *110*, 391.
(40) Paramonov, G. K.; Naundorf, H.; Kühn, O. *Eur. J. Phys. D* **2001**, *14*, 205.
(41) Makri, N.; Miller, W. H. *J. Chem. Phys.* **1987**, *87*, 5781.
(42) Beck, M. H.; Jäckle, A.; Worth, G. A.; Meyer, H.-D. *Phys. Rep.* **2000**, *324*, 1.
(43) Naundorf, H.; Worth, G. A.; Meyer, H.-D.; Kühn, O. *J. Phys. Chem. A* **2002**, *106*, 719.
(44) Korolkov, M. V.; Manz, J.; Paramonov, G. K. *Adv. Chem. Phys.* **1997**, *101*, 327.
(45) Došlić, N.; Sundermann, K.; González, L.; Mó, O.; Giraud-Girard, J.; Kühn, O. *Phys. Chem. Chem. Phys.* **1999**, *1*, 1249.
(46) Heyne, K.; Stenger, J.; Dreyer, J.; Nibbering, E. T. J.; Elsaesser, T. Max Born Institute. Unpublished work, 2003.
(47) Frisch, M. J.; Trucks, G. W.; Schlegel, H. B.; Scuseria, G. E.; Robb, M. A.; Cheeseman, J. R.; Zakrzewski, V. G.; Montgomery, J. A., Jr.; Stratmann, R. E.; Burant, J. C.; Dapprich, S.; Millam, J. M.; Daniels, A. D.; Kudin, K. N.; Strain, M. C.; Farkas, O.; Tomasi, J.; Barone, V.; Cossi, M.; Cammi, R.; Mennucci, B.; Pomelli, C.; Adamo, C.; Clifford, S.; Ochterski, J.; Petersson, G. A.; Ayala, P. Y.; Cui, Q.; Morokuma, K.; Malick, D. K.; Rabuck, A. D.; Raghavachari, K.; Foresman, J. B.; Cioslowski, J.; Ortiz, J. V.; Stefanov, B. B.; Liu, G.; Liashenko, A.; Piskorz, P.; Komaromi, I.; Gomperts, R.; Martin, R. L.; Fox, D. J.; Keith, T.; Al-Laham, M. A.; Peng, C. Y.; Nanayakkara, A.; Gonzalez, C.; Challacombe, M.; Gill, P. M. W.; Johnson, B. G.; Chen, W.; Wong, M. W.; Andres, J. L.; Head-Gordon, M.; Replogle, E. S.; Pople, J. A. *Gaussian 98*, revision A.11; Gaussian, Inc.: Pittsburgh, PA, 1998.
(48) Simperler, A.; Mikenda, W. *Chem. Mon.* **1997**, *128*, 969.
(49) Fores, M.; Duran, M.; Sola, M. *Chem. Phys.* **1998**, *234*, 1.
(50) Rodríguez-Santiago, L.; Sodupe, M.; Oliva, A.; Bertran, J. *J. Am. Chem. Soc.* **1999**, *121*, 8882.
(51) Fores, M.; Duran, M.; Sola, M. *Chem. Phys.* **2000**, *260*, 53.
(52) Benderskii, V. A.; Vetoshkin, E. V.; Trommsdorff, H. P. *Chem. Phys.* **1998**, *234*, 153.
(53) Worth, G. A.; Meyer, H.-D.; Cederbaum, L. S. *J. Chem. Phys.* **1996**, *105*, 4412.
(54) Worth, G. A.; Beck, M.; Jäckle, A.; Meyer, H.-D. *The MCTDH Package*, version 8.3; University of Heidelberg: Heidelberg, Germany, 2002.
(55) Došlić, N.; Kühn, O.; Manz, J. *Ber. Bunsen-Ges. Phys. Chem.* **1998**, *102*, 292.
(56) Naundorf, H.; Sundermann, K.; Kühn, O. *Chem. Phys.* **1999**, *240*, 163.
(57) Schmidt, B.; et al. *WavePacket 3.0*: *A Program Package for Wavepacket Propagation and Time-Dependent Spectroscopy*; Free University: Berlin, 2003.